Dalton Transactions

Formation of a uranyl hydroxide hydrate via hydration of $[(UO_2F_2)(H_2O)]7 *4H_2O$

Journal:	*Dalton Transactions*
Manuscript ID	DT-ART-07-2019-002835.R1
Article Type:	Paper
Date Submitted by the Author:	12-Aug-2019
Complete List of Authors:	Kirkegaard, Marie; Oak Ridge National Laboratory, Nuclear Nonproliferation Division; University of Tennessee Knoxville, Bredesen Center for Interdisciplinary Research and Graduate Education Spano, Tyler; Oak Ridge National Laboratory, Nuclear Nonproliferation Division Ambrogio, Michael; Oak Ridge National Laboratory, Nuclear Nonproliferation Division Niedziela, J; Oak Ridge National Laboratory, Nuclear Nonproliferation Division Miskowiec, Andrew; Oak Ridge National Laboratory, Nuclear Nonproliferation Division Shields, Ashley; Oak Ridge National Laboratory, Nuclear Nonproliferation Division Anderson, Brian; Oak Ridge National Laboratory, Nuclear Nonproliferation Division; University of Tennessee Knoxville, Bredesen Center for Interdisciplinary Research and Graduate Education

Journal Name

ARTICLE TYPE

Cite this: DOI: 00.0000/xxxxxxxxxx

Formation of a uranyl hydroxide hydrate via hydration of $[(UO_2F_2)(H_2O)]_7 \cdot 4H_2O$†

Marie C. Kirkegaard,[a,b] Tyler L. Spano,[a] Michael W. Ambrogio,[a] J. L. Niedziela,[a] Andrew Miskowiec,[a] Ashley E. Shields,[a] and Brian B. Anderson[a,b,*]

Received Date
Accepted Date

DOI: 00.0000/xxxxxxxxxx

Hydrated uranyl fluoride, $[(UO_2F_2)(H_2O)]_7 \cdot 4H_2O$, is not stable at elevated water vapor pressure, undergoing a complete loss of fluorine to form a uranyl hydroxide hydrate. Powder x-ray diffraction data of the resultant uranyl hydroxide species is presented for the first time, along with Raman and infrared (IR) spectra. The new uranyl hydroxide species is structurally similar to the layered uranyl hydroxide hydrate minerals schoepite and metaschoepite, but has a significantly expanded interlayer spacing (c=15.12 vs. 14.73 Å), suggesting that additional H_2O molecules may be present between the uranyl layers. Comparison of the Raman and IR spectra of this new uranyl hydroxide hydrate and synthetic metaschoepite ($[(UO_2)_4O(OH)_6] \cdot 5H_2O$) suggests that the equatorial environment of the uranyl ion may differ and that H_2O molecules in the new species participate in stronger hydrogen bonds. In addition, the interlayer spacing of both this new uranyl hydroxide species and synthetic metaschoepite is shown to be sensitive to the environmental humidity, contracting and re-expanding with desiccation and rehydration. Structural distinction between the new uranyl hydroxide species and synthetic metaschoepite is confirmed by a comparison of the thermal behavior; unlike metaschoepite, the new hydrate does not form $\alpha - UO_2(OH)_2$ upon dehydration.

1 Introduction

We previously demonstrated that hydrated uranyl fluoride, $[(UO_2F_2)(H_2O)]_7 \cdot 4H_2O$, is not stable at elevated water vapor pressure but rather transforms into a uranyl hydroxide hydrate and eventually, a uranyl peroxide hydrate.[1] At the time, the uranyl hydroxide product was identified as such based on Raman and scanning electron microscopy with energy-dispersive x-ray spectroscopy (SEM-EDS) data consistent with known uranyl hydroxide species.[1] In particular, Raman peaks at 845 cm^{-1} and 550 cm^{-1} were noted to be consistent with other studies of uranyl hydroxide hydrates.[2,3] However, vibrational spectra of uranyl hydroxide species vary significantly in the literature,[4] complicating a more rigorous characterization of the hydration product based on vibrational spectroscopy alone. This motivated a follow-up study with structural characterization via powder x-ray diffraction (XRD), necessitating the production of a bulk sample of the new material.

In the absence of single-crystal diffraction data, this new uranyl hydroxide hydrate can be characterized in part via comparison to known uranyl hydroxide structures like the mineral schoepite, $[(UO_2)_4(O)(OH)_6] \cdot 6H_2O$,[5,6] (Figure 1) and its dehydration product metaschoepite, $[(UO_2)_4(O)(OH)_6] \cdot 5H_2O$[7]. These species have similar structures, and differ primarily in the number and arrangement of interlayer H_2O molecules.[7,8] Despite structural similarities, schoepite and metaschoepite can be distinguished by their a and b lattice parameters.[4,7] A survey of crystallographic studies of schoepite[5,6,9–11] and metaschoepite[4,7,11–13] finds that while the a and b lattice parameters are both statistically distinct (p-value=$5.5 * 10^{-5}$ and 0.026, respectively), the c lattice parameter, which defines the interlayer spacing, is not statistically distinct (p-value=0.48). This is illustrated in Figure 2. Thus, removal of interlayer H_2O molecules in the transition from schoepite to metaschoepite does not change the interlayer spacing.

An additional uranyl hydroxide hydrate mineral, paraschoepite, was identified by Schoep and Stradiot in 1947[14] and later partially characterized via powder XRD by Christ and Clark in 1960 as a component of a mixed-phase mineral sample.[11] No further evidence of paraschoepite has been presented. The existence of paraschoepite was more recently questioned by

[a] National Security Sciences Directorate, Oak Ridge National Laboratory, 1 Bethel Valley Rd, Oak Ridge, Tennessee, USA.
[b] Bredesen Center for Interdisciplinary Research and Graduate Education, University of Tennessee, Knoxville, USA.
* E-mail: andersonbb@ornl.gov

† Electronic Supplementary Information (ESI) available: XRD patterns of initial material, vibrational spectral fits, computationally predicted vibrational spectra, additional in-situ XRD data. See DOI: 00.0000/00000000.

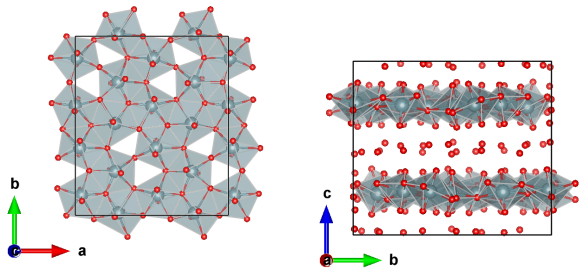

Fig. 1 (Left) Top-down and (Right) side views of the crystal structure of schoepite, $[(UO_2)_4(O)(OH)_6]\cdot 6H_2O$, as determined by Finch et al.[5] Oxygen atoms in between the layers of uranyl polyhedra correspond to H_2O molecules; hydrogen atoms are omitted as their location was not solved experimentally.

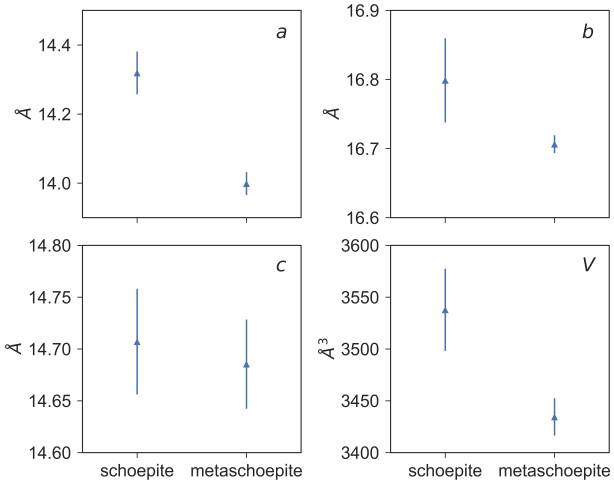

Fig. 2 Average lattice parameters reported from structural characterization of schoepite[5,6,9–11] and metaschoepite[4,7,11–13]. Error bars are $\pm\sigma$. For consistency, lattice parameters for both schoepite and metaschoepite are defined as reported for schoepite, which belongs to the *Pbcn* space group. The *c* parameter is normal to the uranyl layers.

Burns et al., who suggested that the extraneous diffraction maxima in a schoepite sample that Christ and Clark assigned to paraschoepite may have been due to crystallographically oriented inclusions of the mixed-valence uranium oxide hydrate ianthinite, $[U_2^{4+}(UO_2)_4O_6(OH)_4(H_2O)_4]\cdot 5H_2O$.[15] Thus, there remains lingering uncertainty over the number of different uranyl hydroxide hydrate species that exist, whether as minerals or produced synthetically. The identification of a uranyl hydroxide hydrate species formed from the hydration of uranyl fluoride is particularly interesting in this light, and further characterization of this species is motivated to elucidate how this species is distinct from other known or predicted species.

2 Experimental Methods

2.1 Material production

Uranyl fluoride starting material was prepared through the hydrolysis of UF_6 ($UF_6 + 2H_2O \longrightarrow UO_2F_2 + 4HF$) in a reaction chamber containing approximately 20% relative humidity (RH) at 23 °C. Uranyl fluoride particulates were collected on silicon plates at the bottom of the chamber. The powder material was then ground and left exposed to silica desiccant beads for two weeks to remove residual surface water. The powder XRD pattern of the resulting pale yellow powder was consistent with the uranyl fluoride hydrate identified by Mikhailov et al.,[16] $[(UO_2F_2)(H_2O)]_7\cdot 4H_2O$ (Figure S1).

Synthetic metaschoepite was produced from the hydration of amorphous UO_3 for comparison to the newly identified uranyl hydroxide species. Uranyl nitrate hexahydrate crystals (depleted, from SPI-Chem) were first ground into a powder and then heated in air at 300 °C for 24 h to produce dark red x-ray–amorphous UO_3. The heat was then reduced to 80 °C, and deionized water was introduced while stirring continuously. After the solution turned bright yellow (approximately 10 min), it was removed from the heat and allowed to evaporate in ambient conditions (approximately 22 °C and 60% RH). Once dry, the bright yellow powder was rinsed twice with deionized water to remove residual nitrates and again allowed to dry at ambient conditions. The XRD pattern of the resulting material (Figure S2) was consistent with synthetic metaschoepite, $[(UO_2)_4O(OH)_6]\cdot 5H_2O$,[7] with a minor component attributable to anhydrous uranyl hydroxide, $UO_2(OH)_2$. Because synthetic metaschoepite was found to be unstable to dehydration at moderate and low humidity,[4] the uranyl hydroxide material was stored in a sealed glass bell jar and exposed to the headspace of a NaCl saturated salt solution, providing approximately 75% RH at ambient temperature (22-23 °C).

2.2 Sample production

Two uranyl fluoride samples were produced by depositing a few milligrams of uranyl fluoride hydrate ($[(UO_2F_2)(H_2O)]_7\cdot 4H_2O$) onto zero-background silicon XRD plates along with a small amount of silicon powder to act as a standard. No solvent was used in the preparation of the XRD plates to prevent dehydration or other alteration of the material. The two plates were then placed on top of mounts in separate sealed plastic containers that were filled with a small amount of a KCl saturated salt solution (83-84% RH). The two samples were stored in two different incubators, set to 25 and 35 °C (±0.5 °C), respectively. Samples were removed from their hydration containers for periodic XRD and Raman analysis, and measurements were carried out under ambient conditions.

2.3 X-ray diffraction

XRD measurements were obtained on a Proto AXRD using Cu K_α radiation (λ=1.5406 Å). Data were collected using a 0.5 mm divergence slit over the angular range 2θ = [10,50] in steps of $\delta 2\theta$ = 0.02°. The total time for each scan ranged from 45 min to 14 h. Where appropriate, Rietveld refinement of XRD data was performed with GSAS II.[17]

2.4 Raman spectroscopy

Raman spectra were collected using an inVia^{TM} micro-Raman spectrometer (Renishaw) with an excitation wavelength of 785 nm and a 1200 l/mm grating (3 cm^{-1} resolution). A low incident laser power of <1.5 μW, corresponding to a power density of <100 W/cm^2 (laser beam waist = 1.28 um), was used because syn-

thetic metaschoepite was previously shown to be very sensitive to alteration via laser heating at higher laser power.[4] Reported spectra are the sum of 50 accumulations, each with a 3 sec exposure time. Prior to analysis and fitting, all Raman spectra were baseline corrected using the asymmetric least squares approach.[18,19] Raman spectra were fit to pseudo-Voigt functions with both Gaussian and Lorentzian components using the *LmFit* curve-fitting package in Python[20].

2.5 Infrared spectroscopy

Infrared (IR) spectra were collected using a Nicolet iS50 FTIR (Thermo Scientific) with a HeNe laser and ABX Automated Beamsplitter (1.5 cm^{-1} resolution). All spectra were collected using a diamond attenuated total reflectance (ATR) attachment, with background spectra first collected on the empty ATR attachment. Reported spectra are the sum of 32 accumulations, each with a 2 sec exposure time. IR spectra were fit to pseudo-Voigt functions with both Gaussian and Lorentzian components using the *LmFit* curve-fitting package in Python[20].

2.6 Density Functional Theory

The relationship between water content and interlayer spacing was explored via complementary Density Functional Theory (DFT) calculations. The full unit cell of schoepite (344 atoms) was optimized using the Perdew–Burke-Ernzerhof (PBE)[21] functional with the plane-wave code VASP[22], in the same manner as previously presented for metaschoepite.[4] Due to the large unit cell, all calculations were performed at the Γ point, with a cut-off energy of 600 eV. Varying numbers of interlayer H_2O molecules were removed from the unit cell, the structure of which was then re-optimized until the forces on each ion were less than 0.001 eV/Å.

3 Results and Discussion

3.1 Formation of uranyl hydroxide via hydration of uranyl fluoride

The transformation of uranyl fluoride hydrate to the previously identified uranyl hydroxide material was monitored by periodically collecting XRD and Raman spectroscopy data on two samples of uranyl fluoride stored at 25 °C/84% RH and 35 °C/83% RH, respectively. Both samples were observed to undergo a chemical transformation upon hydration, as characterized by both XRD and Raman spectroscopy. At 25 °C and 84% RH (P_{H_2O}=2.67 kPa), this hydration reaction proceeded very slowly over the course of the 140-day experiment, as visible from both the XRD pattern and the uranyl stretching region of the Raman spectrum (Figure 3). At 35 °C and 83% RH (P_{H_2O}=4.67 kPa), however, a complete transformation occurred over this time frame, as shown in Figure 4. The changes in the Raman spectra were consistent with the reaction from uranyl fluoride to a uranyl hydroxide hydration product previously identified in hydrated $[(UO_2F_2)(H_2O)]_7 \cdot 4H_2O$ particles, although the hydration reaction was found to occur much more slowly in the bulk. For comparison, complete transformation of uranyl fluoride particles to uranyl hydroxide at 75% RH at ambient temperature (20-22 °C) was observed to take approximately 50 days,[1] while the same reaction had barely progressed after 140 days at 84% RH and 25 °C for the bulk sample. Increasing the temperature was found to significantly accelerate the reaction such that conversion of a bulk sample was attainable in several months (Figure 4).

Collection of multiple micro-Raman spectra during each analysis revealed that the sample did not hydrate homogeneously. This is illustrated in Figure 5. While the initial uranyl fluoride material was found to be homogeneous as characterized via Raman spectroscopy, formation of the uranyl hydroxide product occurred more rapidly in some regions than others, potentially due to variations in the surface morphology of the sample. This is consistent with prior observations that the rate of hydration varied somewhat among different particles on the same sample.[1] After 140 days, the sample hydrated at 35 °C had completely transformed from uranyl fluoride to uranyl hydroxide as evidenced from the XRD data (Figure 4). At this point, as shown in Figure 5, the Raman spectra were once again consistent across the sample, with no evidence of remaining $[(UO_2F_2)(H_2O)]_7 \cdot 4H_2O$. There was also no evidence of the uranyl peroxide species that was previously observed to form in hydrated particulate samples, which would be evidenced by a peroxo stretching mode near 865 cm^{-1}.[1,24] The absence of this second hydration product of uranyl fluoride is not surprising given the much slower hydration rate observed for the bulk vs. particle samples.

Particles of the uranyl hydroxide hydration product formed after 140 days of hydration were also analyzed via SEM-EDS. These particles were transferred from the initial silicon XRD plate to another silicon substrate prior to EDS analysis. Multiple particles were analyzed on the sample and found to be relatively consistent. Figure 6 shows a representative EDS spectrum. Uranium, oxygen, and silicon (from the background) are identified as the major elemental components, as expected. A small peak near 0.68 keV is attributed to residual fluorine, which is not unexpected since this material was produced from the hydration of uranyl fluoride and likely still contains a minor component of uranyl fluoride. This peak would be expected to disappear upon further hydration.

3.2 Structure of the uranyl hydroxide hydration product

As shown in Figure 4, after 140 days of hydration at 35 °C and 84% RH, the $[(UO_2F_2)(H_2O)]_7 \cdot 4H_2O$ starting material has undergone an essentially complete conversion to a new species. The diffraction maxima of this hydration species are similar to those expected of schoepite, $[(UO_2)_4(O)(OH)_6] \cdot 6H_2O$. The most notable difference between the two patterns is a shift in the (002) and (004) reflections near $2\theta = 12^\circ$ and 24°, respectively, indicative of an expanded layer spacing. Rietveld refinement was used to determine the lattice parameters of the uranyl hydroxide hydration product using schoepite as an initial structure (Figure S3). The refined lattice parameters are shown in Table 1 compared to other uranyl hydroxide hydrates. The primary distinction of the uranyl hydroxide hydration product from the known structures schoepite and metaschoepite is an expanded c lattice parameter (the c direction has been redefined to be perpendicular to uranyl sheets in both schoepite and metaschoepite). This lattice parameter is 15.1214 Å in the uranyl hydroxide hydration product, compared

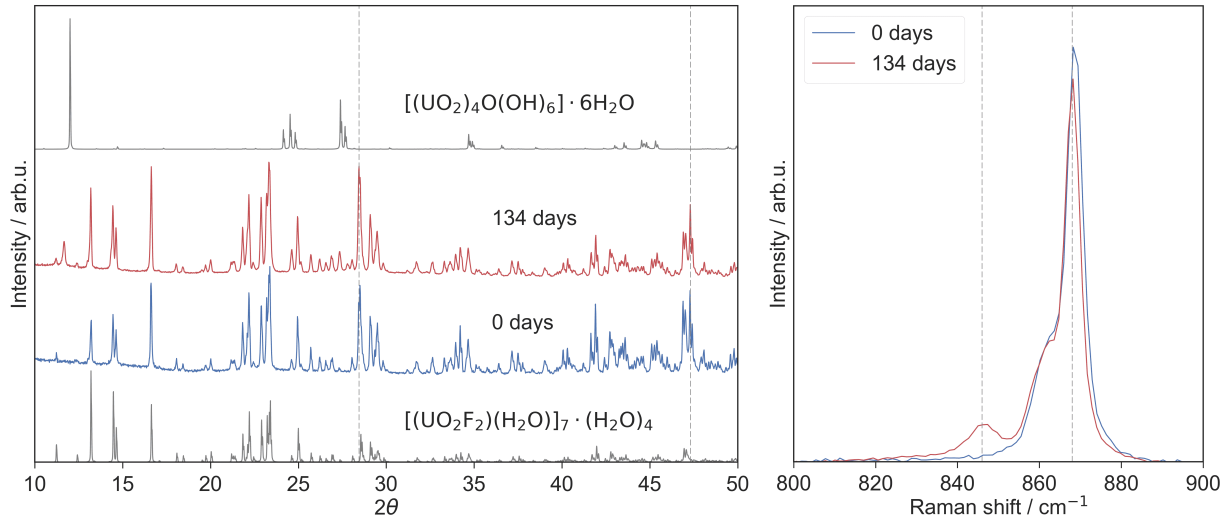

Fig. 3 (Left) XRD patterns (λ=1.5406 Å) over time of a sample of $[(UO_2F_2)(H_2O)]_7 \cdot 4H_2O$ stored at 84% RH at 25 °C (P_{H_2O}=2.67 kPa) compared to the expected patterns of uranyl fluoride hydrate ($[(UO_2F_2)(H_2O)]_7 \cdot 4H_2O$, PDF 01-074-3593[23]) and schoepite ($[(UO_2)_4(O)(OH)_6] \cdot 6H_2O$, PDF 00-050-1601[23]). Dashed lines show the position of peaks corresponding to the silicon standard added to the sample. (Right) The uranyl stretching region of the Raman spectrum of the same sample over time. Spectra are normalized by the area under the curve in the region shown. Dashed lines at 868 and 846 cm^{-1} highlight the location of the dominant uranyl stretching modes of $[(UO_2F_2)(H_2O)]_7 \cdot 4H_2O$ and the uranyl hydroxide hydration product, respectively.

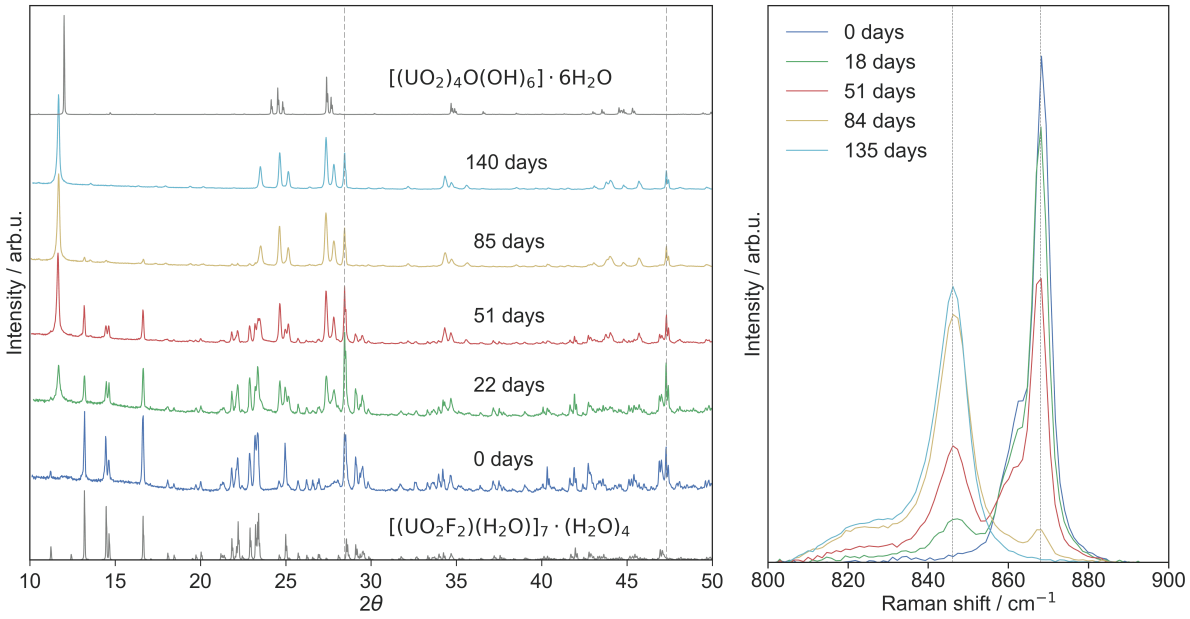

Fig. 4 (Left) XRD patterns (λ=1.5406 Å) over time of a sample of $[(UO_2F_2)(H_2O)]_7 \cdot 4H_2O$ stored at 83% RH at 35 °C (P_{H_2O}=4.67 kPa) compared to the expected patterns of uranyl fluoride hydrate ($[(UO_2F_2)(H_2O)]_7 \cdot 4H_2O$, PDF 01-074-3593[23]) and schoepite ($[(UO_2)_4O(OH)_6] \cdot 6H_2O$, PDF 00-050-1601[23]). Dashed lines show the position of peaks corresponding to the silicon standard added to the sample. (Right) The uranyl stretching region of the Raman spectrum of the same sample over time. Spectra are normalized by the area under the curve in the region shown. Dashed lines at 868 and 846 cm^{-1} highlight the location of the dominant uranyl stretching modes of $[(UO_2F_2)(H_2O)]_7 \cdot 4H_2O$ and the uranyl hydroxide hydration product, respectively.

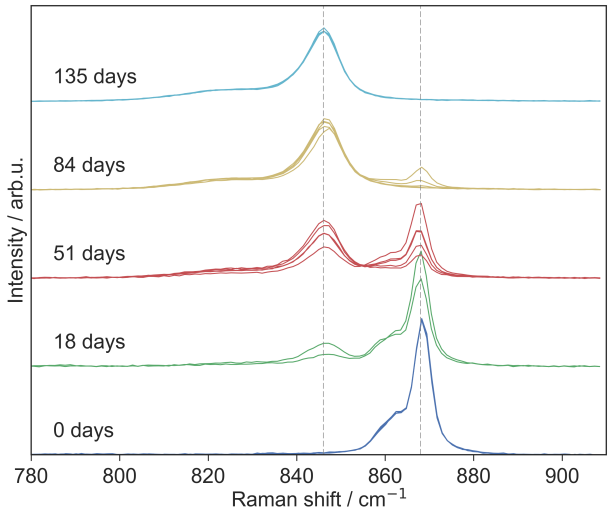

Fig. 5 The uranyl stretching region of the Raman spectrum over time of a sample of $[(UO_2F_2)(H_2O)]_7 \cdot 4H_2O$ stored at 83% RH at 35 °C (P_{H_2O}=4.67 kPa). Five Raman spectra were collected from random regions of the sample on each day, with the exception of after 18 days of hydration, when only two spectra were collected. Spectra are normalized by the area under the curve in the region shown. Dashed lines at 868 and 846 cm^{-1} highlight the location of the dominant uranyl stretching modes of $[(UO_2F_2)(H_2O)]_7 \cdot 4H_2O$ and the uranyl hydroxide hydration product, respectively.

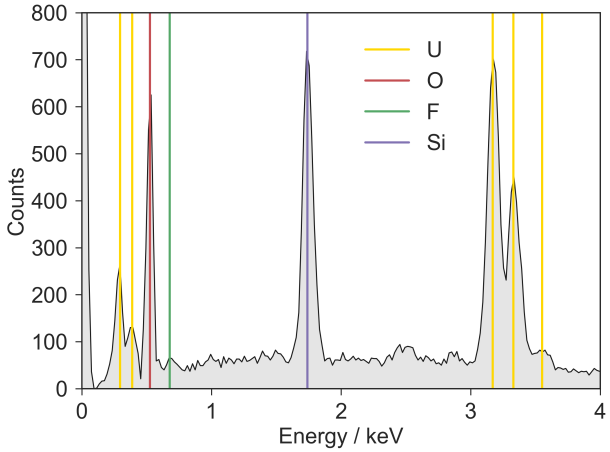

Fig. 6 SEM-EDS spectrum of a representative particle of the uranyl hydroxide hydration product on a silicon substrate. Peaks are attributed to U, O, F, and Si as shown.

with approximately 14.73 Å in both schoepite and metaschoepite.

The expanded layer spacing in the uranyl hydroxide hydration product relative to schoepite or metaschoepite is reminiscent of the proposed mineral paraschoepite.[14] As shown in Figure 7, the diffraction maxima of the uranyl hydroxide hydration product match reflections of paraschoepite reported by Christ and Clark from a mixed-phase mineral sample.[11] While ianthinite has a similarly expanded layer spacing relative to schoepite and metaschoepite, the presence of ianthinite in this sample seems unlikely due to lack of prominent peaks in the 2θ=26–27° region of the powder diffraction pattern. The diffraction maxima of the uranyl hydroxide hydration product cannot be attributed to a mixture of schoepite and its dehydration products either. The sharpness of the diffraction maximum at 2θ=12° as well as the homogeneity of collected Raman spectra after complete hydration suggests that the uranyl hydroxide hydration product is a single phase. While it is impossible to confirm whether the uranyl hydroxide hydration product is a synthetic analog of paraschoepite, the existence of a uranyl hydroxide hydrate with similarly expanded layer spacing adds weight to claims that this mineral may exist.

There is additional evidence of synthetic uranyl hydroxide hydrate species with expanded layer spacing. Weller et al. found that a crystal of metaschoepite cooled to 150 K and then warmed to room temperature and left at ambient conditions for several months transformed to a distinct structure with an expanded layer spacing (Table 1). A full structural solution of this species was not made, and the relationship between metaschoepite and this distinct species is unclear. However, the composition of the aged sample was determined to be $UO_3 \cdot 2.25H_2O$, with more water per unit cell than metaschoepite, which has the empirical formula $UO_3 \cdot 2H_2O$.[7] This suggests that the layer spacing expands to incorporate additional H_2O molecules. Since the uranyl hydroxide hydration product in this work was formed at high RH, it may have a similarly elevated water content in comparison to schoepite and metaschoepite.

3.3 Hydration of synthetic metaschoepite

The hypothesis that the uranyl hydroxide hydration product may contain more interlayer H_2O molecules than schoepite and metaschoepite raises the question of whether or not it is possible to form this species via the hydration of these known materials. Synthetic metaschoepite can be readily produced for such a hydration experiment. It was demonstrated previously that the structure of bulk synthetic metaschoepite is not altered by long-term exposure to a 75% RH environment.[4] To further hydrate synthetic metaschoepite, an XRD sample was stored in a container with a KNO_3 saturated salt solution at 35 °C (91% RH, P_{H_2O}=5.11 kPa) for 127 days. XRD and Raman data were collected periodically over this time period. While collecting XRD data necessitated removing the sample from the hydrating environment, scans were limited to 45 min to minimize potential dehydration during measurement.

Figure 8 shows the XRD pattern of this sample over time. There is no evidence of a significant change in interlayer spacing. The interlayer spacing was actually observed to contract slightly between 0 and 70 days of hydration, although this was likely the result of slight dehydration during measurement. This finding led to a more thorough investigation of the humidity dependence of the interlayer spacing discussed in this work.

While the XRD pattern of this hydrated sample was not indicative of a major structural change, Raman spectra collected on the sample over time showed changes in the uranyl stretching region (Figure 9). In particular, the initial uranyl stretching mode near 868 cm^{-1} was observed to redshift significantly upon hydration, while uranyl stretching modes at 845 cm^{-1} and below were observed to broaden slightly but did not shift notably. As demonstrated in Figure 9, collection of multiple spectra in differ-

Table 1 Lattice parameters obtained from Rietveld refinement of the XRD pattern of the uranyl hydroxide hydration product compared to other uranyl hydroxide hydrates. Lattice parameters are oriented so that the c-axis is perpendicular to the uranyl sheets. All distances are in Å, and all lattice angles are 90°.

Sample	a	b	c
Schoepite[5]	14.337(3)	16.813(5)	14.731(4)
Synthetic metaschoepite[7]	14.050(2)	16.709(2)	14.7291(2)
Aged metaschoepite[7a]	14.112	16.768	15.143
Synthetic metaschoepite[4]	13.9828(4)	16.7038(5)	14.6964(5)
Paraschoepite[11b]	14.12	16.83	15.22
Uranyl hydroxide product, this work	14.1457(7)	16.7757(8)	15.1214(9)

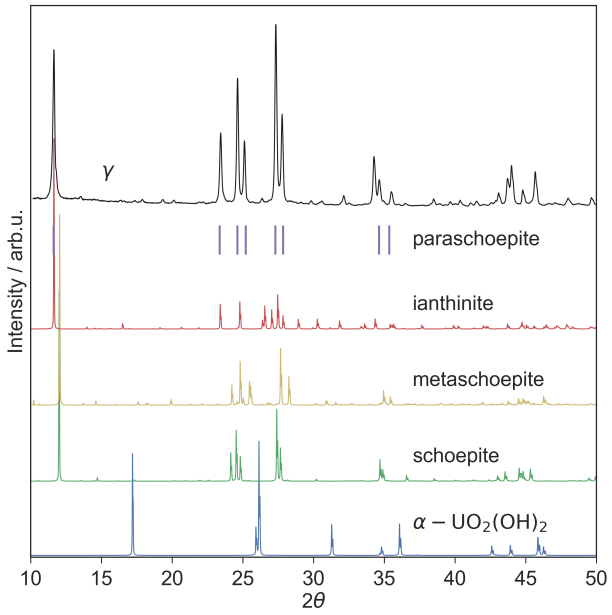

Fig. 7 XRD pattern (λ=1.5406 Å) of the uranyl hydroxide hydration product compared to the reflections reported for the debated species "paraschoepite"[11] (also referred to as schoepite-III by Christ and Clark) and the known patterns of ianthinite[15] (PDF 04-014-4069[23]), metaschoepite[7] (PDF 04-011-3920[23]), schoepite[5] (PDF 00-050-1601[23]), and anhydrous uranyl hydroxide[25] (α−$UO_2(OH)_2$, PDF 04-007-5373[23]) .

ent regions of the sample on each date of analysis revealed that these changes did not occur homogeneously across the sample.

No changes were observed in the lower energy region (100-600 cm^{-1}) of the Raman spectrum, suggesting that the equatorial environment of the uranyl ion remains unchanged.[4] Instead, it appears that the local environment of a subset of the uranyl ions changes without any effect on the long-range structure or equatorial bonding. This is consistent with a change in the interlayer water structure that strengthens hydrogen bonding interactions to some of the uranyl oxygens. The nature of these changes deserves additional study, but is beyond the scope of this paper.

3.4 Comparison of the vibrational spectra of the uranyl hydroxide hydration product and synthetic metaschoepite

The full Raman spectrum of the uranyl hydroxide hydration product, obtained on the same material on which XRD data were collected, is shown in Figure 10. The Raman spectrum of synthetic metaschoepite, as previously reported,[4] is shown for comparison. A list of the Raman peaks and their assignments is shown in Table 2; pseudo-Voigt fits are included in the ESI. The uranyl stretching region of the Raman spectrum of the uranyl hydroxide hydration product is characterized by a dominant peak at 846 cm^{-1} with a shoulder centered at 830 cm^{-1}. The presence of two uranyl stretching modes indicates the existence of multiple uranyl ion environments that may differ by equatorial coordination or hydrogen bonding interactions.[26] Additional Raman peaks appear at 555, 515, 459, 400, 330, 257, 199, 158, and 127 cm^{-1}. Many of the peaks in this lower-energy region are distinct from those observed in synthetic metaschoepite, suggesting that the arrangement of equatorial hydroxy and oxide ligands in the two structures may differ. This potentially explains why the uranyl hydroxide hydration product cannot be formed via the hydration of synthetic metaschoepite, as discussed in the previous section.

IR spectroscopy was performed to assess higher energy water and hydroxy related modes. These modes were not visible in the Raman spectrum due to the low incident laser power used to avoid unintentionally altering the sample via laser heating and because water is a weak Raman scatterer. Figure 11 shows the IR spectrum of the uranyl hydroxide hydration product, again compared to that of synthetic metaschoepite.[4] Pseudo-Voigt fits are again included in the ESI; a list of IR peaks and their assignments appears in Table 2. OH stretching modes appear between 2500 and 3700 cm^{-1}. The 3569 and 3483 cm^{-1} peaks are attributed to the OH stretching mode of interlayer H_2O molecules, while the remaining peaks are attributed to the OH stretching mode of hydroxy ligands. The presence of multiple stretching modes for both water and hydroxy groups suggests that some water and hydroxy ligands in the structure participate in stronger hydrogen bonding than others.[27] In general, the OH stretching modes in the uranyl hydroxide hydration product are slightly redshifted compared to synthetic metaschoepite, suggesting the presence of stronger hydrogen bonds.[27] Stronger hydrogen bonding also explains the broadening of peaks between 3400 and 3600 cm^{-1} relative to metaschoepite.

The peak at 1624 cm^{-1} is attributed to the bending mode of the interlayer H_2O molecules. The frequency of this mode is consistent with the frequency of the same mode in synthetic metaschoepite. However, the δ(U−O−H) bending mode is blueshifted in the uranyl hydroxide hydration product (1043 cm^{-1}) compared to

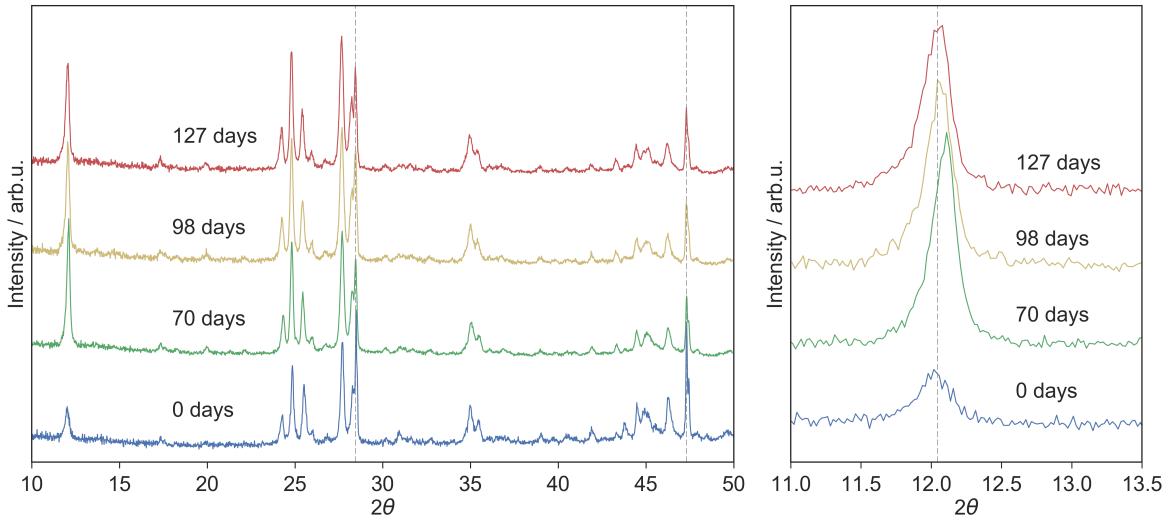

Fig. 8 (Left) XRD pattern (λ=1.5406 Å) of synthetic metaschoepite upon increasing time spent exposed to 91% RH at 35 °C. (Right) Expanded view of the (002) reflection. The dashed line at 2θ=12.043 corresponds to the previously measured value for synthetic metaschoepite (PDF 04-011-3920[23]).[7]

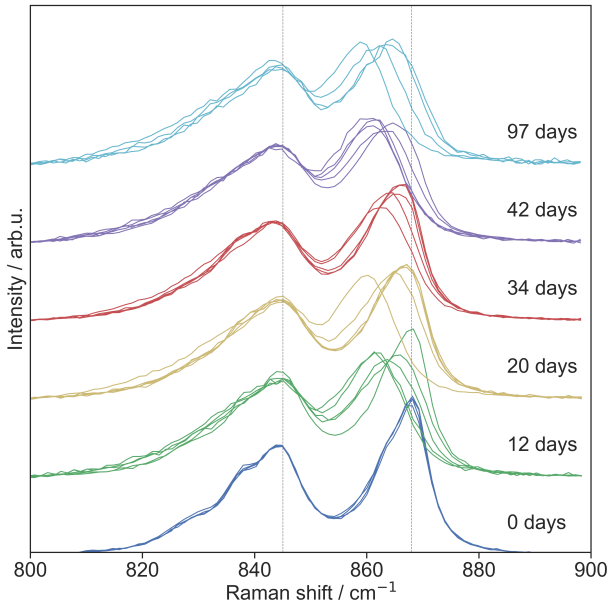

Fig. 9 Raman spectra collected on a sample of synthetic metaschoepite equilibrated for increasing amounts of time in a 95% RH, 35 °C environment. The multiple spectra at each point of hydration correspond to Raman spectra collected on different regions of the sample on the same day. Dashed lines at 868 and 845 cm^{-1} show the initial location of the two dominant uranyl stretching modes.

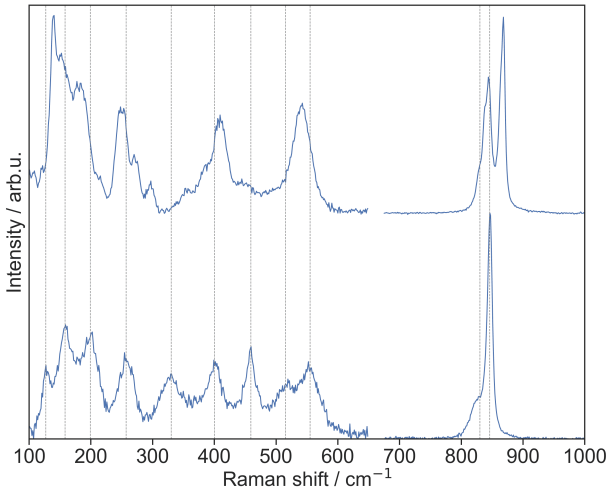

Fig. 10 Comparison of the Raman spectrum of the uranyl hydroxide hydration product (bottom) and synthetic metaschoepite (top). The lower energy region of the spectra is scaled by a factor of five. Dashed lines show the location of peaks in the uranyl hydroxide hydration product (Table 2).

synthetic metaschoepite (1005 cm^{-1}). Based on a comparison of the computationally predicted vibrational spectra of schoepite and metaschoepite (Figure S6), this mode is demonstrated to be the most sensitive to differences in the interlayer water structure and hydrogen bonding network.

A peak at 1423 cm^{-1} in the experimental IR spectrum cannot be assigned. A much smaller peak in this region was noted previously in the IR spectrum of synthetic metaschoepite.[4] Since no peaks were predicted in this region in the computational study of metaschoepite, this peak, along with a small peak at 1335 cm^{-1}, was previously attributed to the presence of impurities in the sample, possibly unreacted uranyl nitrate.[4] However, the presence of the peak at 1423 cm^{-1} in the present study cannot be attributed to uranyl nitrate, since uranyl nitrate was not used in the synthesis. Curiously, a peak near 1400 cm^{-1} was also noted by Urbanec and Cejka in a natural sample of schoepite, although it was not assigned.[28] The energy of this peak is similar to that of the ν_3 vibrational mode of the carbonate ion in the uranyl carbonate minerals rutherfordine and sharpite.[28] However, the absence of a symmetric carbonate stretching mode in the Raman spectrum near 1000-1100 cm^{-1}[29] and lack of carbon signal in the EDS spectrum (Figure S6) suggests that this peak cannot be attributed to the carbonate group. The origin of this peak thus remains unknown and deserves further study.

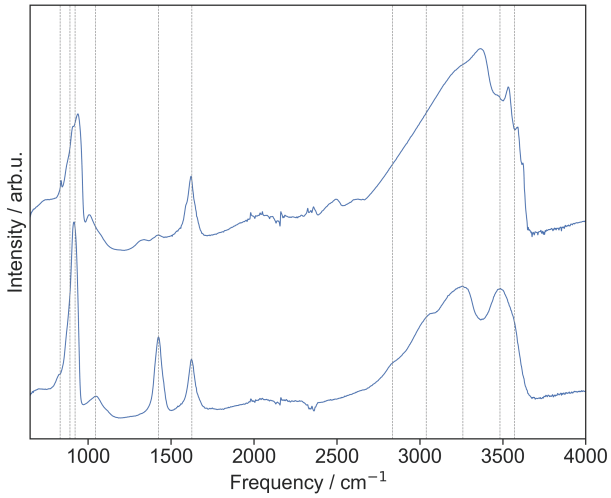

Fig. 11 Comparison of the IR spectrum of the uranyl hydroxide hydration product (bottom) and synthetic metaschoepite (top). Dashed lines show the location of peaks in the uranyl hydroxide hydration product (Table 2).

The uranyl stretching region of the IR spectrum can be fit to three curves at 921, 890, and 830 cm^{-1}. The peaks at 921 and 890 cm^{-1} are assigned to asymmetric uranyl stretching modes. The presence of two modes again indicates multiple uranyl environments. The peak in the IR spectrum at 830 cm^{-1} matches the location of the uranyl stretching shoulder in the Raman spectrum. Hydrogen bonding interactions are known to break the symmetry of the uranyl ion, causing a symmetric stretching mode to appear in the IR spectrum.[30] We thus tentatively assign this peak to the symmetric stretch of uranyl ions that are characterized by strong hydrogen bonding interactions with interlayer H_2O molecules. The corresponding asymmetric mode appears at 890 cm^{-1}. In contrast, uranyl ions that are not characterized by strong hydrogen bonding have a symmetric stretching mode at 846 cm^{-1} and asymmetric stretching mode at 921 cm^{-1}.

3.5 Humidity dependence of uranyl hydroxide hydrates

In a previous study of synthetic metaschoepite,[4] variation was noted in the crystal structure as determined by XRD as a function of the environmental conditions of the sample. In particular, the interlayer spacing was demonstrated to be sensitive to the RH during the sample study. In-situ humidity-controlled XRD experiments were carried out to further probe this behavior. Figure 12 shows the interlayer spacing, determined from the position of the (002) reflection, as a sample of synthetic metaschoepite was exposed to increasing humidity at 30 °C. The interlayer spacing is clearly humidity dependent, increasing by roughly 0.025 Å as the RH was increased from 40 to 60%. Expansion of the layer spacing occured rapidly as the humidity was increased, and remained fairly stable over 12 h at each humidity level. The interlayer spacing determined at 40% RH (∼7.384 Å) is still expanded relative to literature values for schoepite and metaschoepite, which range between 7.31 and 7.375 Å[5,6,9–11], and 7.3065 and 7.365 Å[4,7,11–13], respectively (Figure S8). However, these values were all measured under undefined ambient RH.

Table 2 Raman and IR spectroscopy peaks for the new uranyl hydroxide species.

IR / cm^{-1}	Raman / cm^{-1}	Assignment
3569		ν(OH) (water)
3482		ν(OH) (water)
3258		ν(OH) (hydroxy)
3037		ν(OH) (hydroxy)
2833		ν(OH) (hydroxy)
1624		$\delta(H_2O)$
1423		???
1043		δ(U−O−H)
921		$\nu_{as}(UO_2^{2+})$
890		$\nu_{as}(UO_2^{2+})$
	846	$\nu_s(UO_2^{2+})$
830	830	$\nu_s(UO_2^{2+})$
	555	$\nu(U{=}O_{eq})$ / ν(U=(OH))
	515	$\nu(U{=}O_{eq})$ / ν(U=(OH))
	459	ν(U=(OH)) / γ(U−(OH)−U)
	400	ν(U=(OH)) / γ(U−(OH)−U)
	330	ν(U=(OH)) / γ(U−(OH)−U)
	257	$\delta(UO_2^{2+})$ / δ(U−(OH)−U)
	199	$\delta(UO_2^{2+})$ / δ(U−(OH)−U)
	158	$\delta(UO_2^{2+})$ / lattice modes
	127	$\delta(UO_2^{2+})$ / lattice modes

The lower limit of the interlayer spacing was explored by desiccating another sample of synthetic metaschoepite under dry air at 30 °C. One hour XRD scans were again collected consecutively. As shown in Figure 13, the interlayer spacing was observed to contact upon desiccation, as indicated by shifts in the (002) and (004) reflections. A rapid re-expansion of the layer spacing occurred when the humidity was increased to 50%. In addition, as the sample was rehydrated at 50% RH for several hours, a second peak became visible at 2θ=11.6°. The position of this peak matches the position of the (002) reflection of the uranyl hydroxide hydration product at 50% RH (see Figure 16), suggesting that a component of the synthetic metaschoepite is converted to a species with an expanded layer spacing consistent with that of the new uranyl hydroxide species. This peak cannot be definitively attributed, however, due to the absence of a corresponding (004) reflection near 2θ=23.43°. It is plausible that desiccation induces some disorder in the uranyl layers such that the hydrogen bonding interactions that link the layers via interlayer H_2O molecules are weakened. This would allow the interlayer to be more easily expanded via absorption of additional H_2O molecules.

The relative stability of the a and b lattice parameters, as well as the observed reversibility of this change in interlayer spacing, suggests that there is no significant structural change in the uranyl layers. The contraction and expansion of the c lattice parameter is presumably due to the removal and replacement of a portion of the interlayer H_2O molecules, explored computationally in the next section.

After the RH was held at 50% RH for 24 h, the desiccation/rehydration cycle was repeated a second time (24 h 0% RH, 24 h 50% RH). The contraction and expansion of the c lattice parameter

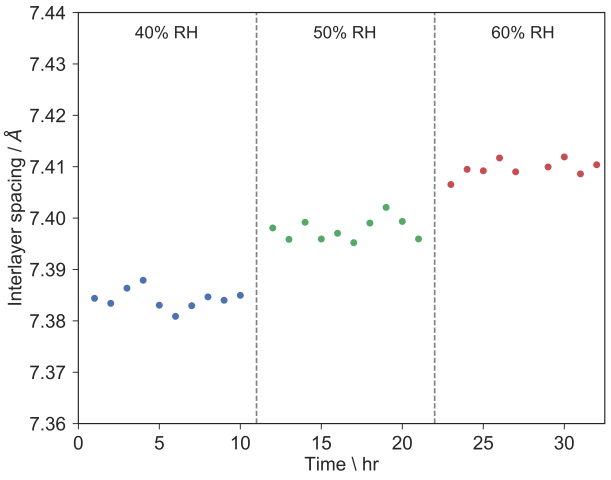

Fig. 12 Interlayer spacing of synthetic metaschoepite at 40%, 50%, and 60% RH at 30 °C, as determined from the position of the (002) reflection. A series of 1 h XRD scans were collected consecutively at each humidity level after equilibrating the sample for 1 h.

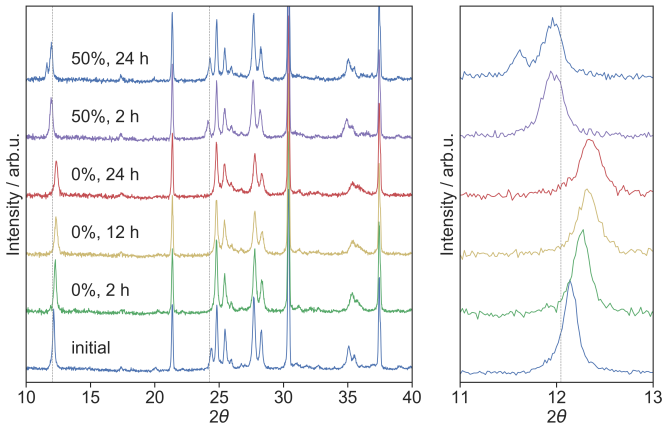

Fig. 13 (Left) XRD pattern (λ=1.5406 Å) of synthetic metaschoepite upon dessication under dry air and then rehydration at 50% RH. Peaks at 2θ=21.36, 30.38, and 37.44° correspond to the LaB_6 standard added to the sample. Dashed lines show the expected location of the (002) and (004) reflections of synthetic metaschoepite (PDF 04-011-3920[23]) at 2θ=12.043° and 2θ=24.2216°. (Right) Expanded view of the (002) reflection.[7]

was found to be reversible over both cycles, as demonstrated in Figure 14, which shows the three lattice parameters over the course of the experiment, as calculated via sequential Rietveld refinement. In contrast, the *b* lattice parameter was found to be very constant throughout the experiment, and while the sudden RH changes seem to have a small effect on the *a* parameter, this effect does not appear to be correlated to the direction of the humidity change and is much smaller in magnitude than the observed variation in the *c* lattice parameter.

The humidity dependence of the uranyl hydroxide hydration product of uranyl fluoride was investigated for comparison to synthetic metaschoepite. An XRD sample of the uranyl hydroxide species was desiccated and rehydrated two times as in the experiment with synthetic metaschoepite, and a similar reversible contraction and expansion of the interlayer spacing was evidenced from shifts in the (002) and (004) reflections (Figure 16). While this species undergoes similar behavior to synthetic metaschoepite, the interlayer spacing can be re-expanded to its initial value upon hydration. This provides additional evidence that the uranyl polyhedral layers are distinct in the two species, and that the newly identified uranyl hydroxide species is not simply extra-hydrated metaschoepite. In addition, while contraction of the interlayer spacing occurred continuously in synthetic metaschoepite, the contraction of the interlayer spacing in the uranyl hydroxide product occurred in two steps, with a discrete shift between (Figure 15). This is proposed to be due to a reorganization of the interlayer water network that occurs after some of the H_2O molecules are removed.

Table 3 compares the refined lattice parameters of synthetic metaschoepite and the uranyl hydroxide product after equilibration at 50% and 0% RH. The *c* lattice parameter of the uranyl hydroxide product remains expanded relative to metaschoepite at 0% RH after the first desiccation cycle. Metaschoepite did not contract as much on the second desiccation cycle, likely due to the introduction of disorder in the metaschoepite uranyl layers, and reached a minimum similar to that of the new uranyl hydroxide species. The *a* and *b* lattice parameters of the uranyl hydroxide product are more sensitive to changes in RH than observed for metaschoepite, shrinking by 0.5 and 0.4%, respectively. This is potentially explained by a less rigid hydrogen bonding network of interlayer H_2O molecules in the uranyl hydroxide hydration product relative to synthetic metaschoepite.

3.6 DFT study to assess structural effect of interlayer H_2O molecules

The removal of a subset of the interlayer H_2O molecules in both synthetic metaschoepite and the uranyl hydroxide hydration product upon short-term desiccation was somewhat unexpected given the strong hydrogen bonding network in uranyl hydroxide hydrates.[4,5,31] Interlayer H_2O molecules are hydrogen bonded not only to each other, but to the hydroxy groups in the uranyl layers as well. The removal of each of these H_2O molecules would thus require the breaking of multiple fairly strong hydrogen bonds.

DFT calculations were carried out to better understand the structural effect of removing a subset of the interlayer H_2O molecules. Schoepite was used in place of metaschoepite for this study because the increased symmetry lessened the computational effort. A series of calculations were carried out in which the schoepite unit cell was re-optimized upon the removal of different numbers of H_2O molecules. The 48 interlayer H_2O molecules in the schoepite unit cell are organized in 12 symmetrically distinct positions. One or more of these 12 groups of H_2O molecules were removed in each calculation. Selection among the 12 groups was random. Because the choice of the specific H_2O molecules removed was expected to affect the resulting interlayer spacing, three separate calculations were run at each water content. An additional two calculations were run with 40 and 44 H_2O molecules removed due to greater variation in the optimized structures at this water content. Structural optimization was done in two steps. Following removal

Table 3 Lattice parameters obtained from Rietveld refinement of synthetic metaschoepite and the uranyl hydroxide hydration product after equilibration at 50% RH and 0% RH (30 °C). Lattice parameters are oriented so that the c-axis is perpendicular to the uranyl sheets. All distances are in Å, and all lattice angles are 90°.

Sample	a	b	c	V
Syn. metaschoepite, 50% RH	13.985(7)	16.684(9)	14.728(8)	3436(2)
Syn. metaschoepite, 0% RH	13.9985(1)	16.7179(1)	14.17017(9)	3316.18(7)
Percent change	0.1%	0.2%	-3.8%	-3.5%
Uranyl hydroxide product, 50% RH	14.156(1)	16.786(2)	15.183(2)	3608.8(5)
Uranyl hydroxide product, 0% RH	14.080(9)	16.716(8)	14.387(5)	3386(2)
Percent change	-0.5%	-0.4%	-5.2%	-6.2%

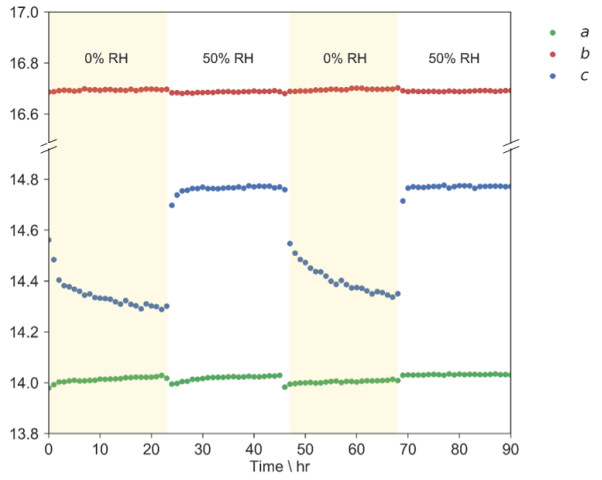

Fig. 14 Lattice parameters of synthetic metaschoepite with the environmental humidity cycled between 0% and 50% RH (30 °C), as determined via sequential Rietveld refinement. One hour XRD scans were collected consecutively throughout the entire experiment, with no delay between.

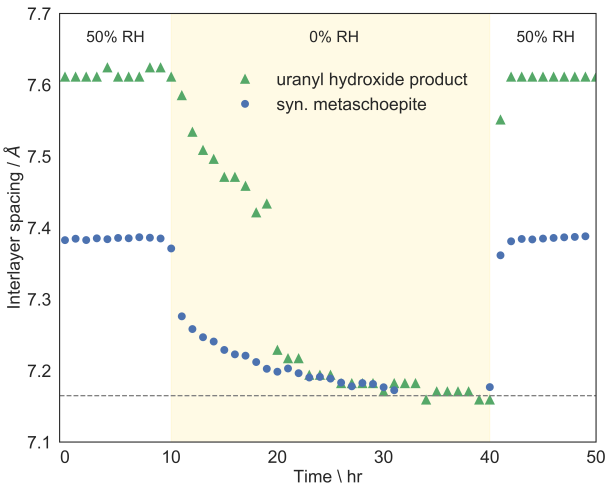

Fig. 15 Interlayer spacing of synthetic metaschoepite (blue circles) and the uranyl hydroxide hydration product (green triangles) over a portion of the rehydration and second desiccation cycle. The RH was set to 50% (at 30 °C) for the first 10 h, and then 0% for the remainder for the time shown. One hour XRD scans were collected consecutively throughout the entire experiment, with no delay between. The interlayer spacing of synthetic metaschoepite was calculated via sequential Rietveld refinement, while the interlayer spacing of the uranyl hydroxide hydration product was calculated from the position of the (002) reflection. The dashed line at 7.165 Å shows the approximate interlayer spacing of both desiccated structures.

of the H_2O molecules, the atomic positions of the remaining atoms were optimized while keeping the lattice parameters fixed. Once the atomic positions were optimized, the lattice parameters were allowed to relax as well, and the atomic positions were optimized for a second time.

The optimized interlayer spacing of each of these calculations is shown in Figure 17 as a function of the number of H_2O molecules removed. As H_2O molecules are removed from the structure, the interlayer contracts as expected. When all or almost all of the interlayer H_2O molecules are removed, the structure collapses in the c-direction and hydrogen bonds form directly between the uranyl oxygens and hydroxy groups in adjacent layers. This full dehydration was previously observed experimentally upon extended exposure to a desiccating environment.[4] This irreversible phase transition is distinct from the reversible contraction and expansion of the layer spacing that occurs more quickly upon changes in the humidity. Figure 17 suggests that the removal of about half of the H_2O molecules in the unit cell of schoepite would result in the 2–3% interlayer contraction observed experimentally, without causing the irreversible collapse of the structure. The average water dissociation energy over all of the calculations was 0.686 eV, likely an underestimate as the PBE functional underestimates the strength of long-range van der Waals interactions.[32,33]

3.7 Thermal stability of uranyl hydroxide hydrates

Differences between the uranyl hydroxide product and synthetic metaschoepite were further assessed by studying the thermal dehydration of each species via in-situ XRD experiments with temperature control. Figure 18 shows the XRD pattern of synthetic metaschoepite with increasing temperature. Two hour XRD scans were collected every 10 °C between 30 and 100 °C, then every 20 °C up to 200 °C, and at 250 and 300 °C. The temperature was ramped 1 °C/min between scans, and the sample was equilibrated at each temperature for 30 min prior to data collection. The dehydration reaction occurs in two steps. Between 30 and 70 °C, the metaschoepite structure contracts in the c direction, while expanding slightly in the a and b directions (Figure 19). At 80 °C and above, a phase transition to anhydrous uranyl hydroxide ($\alpha-UO_2(OH)_2$) occurs.

The same in-situ XRD experiment was repeated with samples of the uranyl hydroxide product to compare the thermal stability

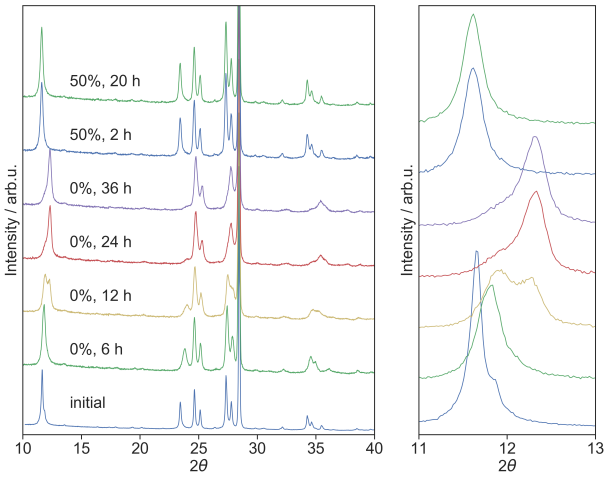

Fig. 16 (Left) XRD pattern (λ=1.5406 Å) of the uranyl hydroxide product upon desiccation under dry air and then rehydration at 50% RH. The peak at 2θ=28.443 corresponds to the Si standard added to the sample. (Right) Expanded view of the (002) reflection.

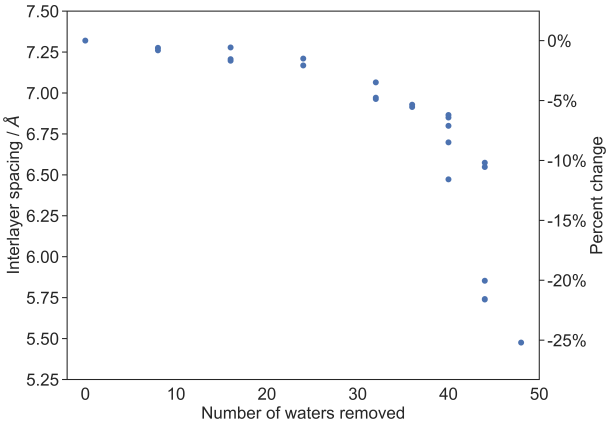

Fig. 17 DFT-optimized interlayer spacing of schoepite with varying number of H_2O molecules removed from the unit cell.

of this new material to synthetic metaschoepite (Figure 20). The dehydration of this species also involves a contraction of the layer spacing similar to that observed upon desiccation, followed by a discrete phase transition that begins around 60 °C. Distinct from synthetic metaschoepite, the *a* and *b* parameters of the new uranyl hydroxide hydration product contract along with the *c* lattice parameter prior to the phase transition (Figure 21), suggesting that the uranyl polyhedra begin to buckle as H_2O molecules are removed. The contraction of the *c* lattice parameter occurs more rapidly between 25 and 40 °C and at the same slower rate as synthetic metaschoepite between 40 and 70 °C. If this species is hydrated relative to synthetic metaschoepite, and there are more H_2O molecules than hydroxy ligands, the excess H_2O molecules cannot form strong hydrogen bonds with hydroxy groups. These H_2O molecules may be removed from the structure more easily, leading to the initial rapid contraction of the interlayer spacing.

While the new uranyl hydroxide species undergoes a discrete phase transition following this contraction, similar to synthetic metaschoepite, the dehydration product is not $\alpha-(UO_2(OH)_2$. This is clearly illustrated in Figure 22, which compares the interlayer spacing of the new uranyl hydroxide species and synthetic metaschoepite as a function of temperature. The dehydration product of the new uranyl hydroxide species has an interlayer spacing between that observed for uranyl hydroxide hydrates and anhydrous uranyl hydroxide that continues to contract upon heating unlike anhydrous uranyl hydroxide. The observed XRD pattern does not match any known uranyl hydroxide species. While Sowder et al. previously noted formation of "partially dehydrated metaschoepite", with an intermediate layer spacing of 5.9 Å after heating synthetic metaschoepite at 105 °C,[34] it is unclear how this species could relate to the dehydration product in this study, which was not produced from metaschoepite.

The expanded interlayer spacing of the dehydration product in this study relative to anhydrous uranyl hydroxide is possibly explained by buckling of the uranyl polyhedra that prevents them from stackly as tightly as observed in anhydrous uranyl hydroxide. The *a* and *b* lattice parameters of the dehydrated structure cannot be adequately determined to evaluate this hypothesis due to the limited number of broad reflections. It is also possible that there exists an interstitial complex between the layers preventing them from collapsing completely. If a subset of the interlayer H_2O molecules were not removed in the phase transition, the interlayer spacing of the dehydration product would be expanded relative to anhydrous uranyl hydroxide. As the layers compress, H_2O molecules could become trapped in the voids between uranyl polyhedra, forming strong hydrogen bonds that could prevent their removal even at high temperature. Above 200 °C, the structure becomes x-ray amorphous, suggesting that the dehydration product does not have the same organized hydrogen bonding scheme as anhydrous uranyl hydroxide. This disorder promotes stability at higher temperatures. The reversibility of this phase transition was not explored in this study but deserves future attention.

4 Conclusions

In summary, uranyl fluoride can be hydrated with water vapor to form a uranyl hydroxide species that is distinct from well-characterized uranyl hydroxide hydrates. The XRD pattern of this species suggests that it is structurally similar to schoepite, but possesses an expanded interlayer spacing. Comparison of the Raman and IR spectra of the new uranyl hydroxide species and synthetic metaschoepite suggest that the uranyl layers in each differ slightly and that the new species is characterized by stronger hydrogen bonding interactions between interlayer H_2O molecules. The distinctions between these two species are clarified by a comparison of their behavior upon desiccation and dehydration. While both the new uranyl hydroxide species and synthetic metaschoepite undergo a reversible contraction and expansion in the *c* direction upon desiccation and rehydration, the fact that the new uranyl hydroxide species retains its expanded layer spacing upon rehydration is further evidence that the uranyl layers are distinct from synthetic metaschoepite (i.e., that these two structures differ in more than just the number of interlayer H_2O molecules). This is further supported by the fact that the new uranyl hydroxide species does not form anhydrous uranyl hydroxide ($\alpha-(UO_2(OH)_2$) upon dehydration, but rather undergoes a phase transition to a dis-

tinct dehydration species with a significantly expanded interlayer spacing.

Further characterization of this new uranyl hydroxide species is necessary to clarify the structure and relationship to the proposed uranyl hydroxide mineral paraschoepite. Presently, further characterization is limited by the slow formation reaction from the hydration of uranyl fluoride. Identification of a different synthetic route to produce this species, or ways to accelerate the known formation mechanism, could enable additional elucidation of the water content and structure via thermogravimetric analysis and neutron scattering experiments.

Conflicts of Interest

There are no conflicts to declare.

Acknowledgments

The authors thank Michael Lance in the Materials Science and Technology Division at Oak Ridge National Laboratory (ORNL) for the use of his Nicolet iS50 FTIR.

This manuscript has been authored by UT-Battelle, LLC, under contract DE-AC05-00OR22725 with the US Department of Energy (DOE). The US government retains and the publisher, by accepting the article for publication, acknowledges that the US government retains a nonexclusive, paid-up, irrevocable, worldwide license to publish or reproduce the published form of this manuscript, or allow others to do so, for US government purposes. DOE will provide public access to these results of federally sponsored research in accordance with the DOE Public Access Plan (http://energy.gov/downloads/doe-public-access-plan). This material is based upon work supported by the US Department of Homeland Security (DHS) under grant award number 2012-DN-130-NF0001. The views and conclusions contained in this document are those of the authors and should not be interpreted as representing the official policies, either expressed or implied, of the US DHS.

Notes and references

1 M. C. Kirkegaard, A. Miskowiec, M. W. Ambrogio and B. B. Anderson, *Inorg. Chem.*, 2018, **57**, 5711–5715.
2 M. Amme, B. Renker, B. Schmid, M. P. Feth, H. Bertagnolli and W. Dobelin, *Journal of Nuclear Materials*, 2002, **306**, 202–212.
3 L. E. Sweet, T. A. Blake, C. H. Henager, S. Hu, T. J. Johnson, D. E. Meier, S. M. Peper and J. M. Schwantes, *Journal of Radioanalytical and Nuclear Chemistry*, 2013, **296**, 105–110.
4 M. C. Kirkegaard, J. L. Niedziela, A. Miskowiec, A. E. Shields and B. B. Anderson, *Inorg. Chem.*, 2019, **58**, 7310–7323.
5 R. J. Finch, M. A. Cooper, F. C. Hawthorne and R. C. Ewing, *Canadian Mineralogist*, 1996, **34**, 1071–1088.
6 J. Plášil, *Journal of Geosciences*, 2018, **63**, 65–73.
7 M. T. Weller, M. E. Light and T. Gelbrich, *Acta Crystallographica Section B*, 2000, **56**, 577–583.
8 R. J. Finch, F. C. Hawthorne and R. C. Ewing, *The Canadian Mineralogist*, 1998, **36**, 831–845.
9 V. Billiet and W. F. de Jong, *Nat. Tijdschr. Ned.-Indie*, 1935, **17**, 157–162.
10 J. Protas, *Bull. Soc. Fr. Miner. Cristal.*, 1959, **82**, 239–272.
11 C. L. Christ and J. R. Clark, *American Mineralogist*, 1960, **45**, 1026–1061.
12 A. L. Klingensmith, K. M. Deely, W. S. Kinman, V. Kelly and P. C. Burns, *American Mineralogist*, 2007, **92**, 662–669.
13 J. Brugger, N. Meisser, B. Etschmannnn, S. Ansermet and A. Pring, *American Mineralogist*, 2011, **96**, 229–240.
14 A. Schoep and S. Stradiot, *Am. Mineral.*, 1947, **32**, 344–350.
15 P. C. Burns, R. J. Finck, F. C. Hawthorne, M. L. Miller and R. C. Ewing, *J. Nucl. Mater.*, 1997, **249**, 199–206.
16 Mikhailov, Yu. N., Gorbunova, Yu. E., Stolyarov, I. P. and Moiseev, I. I., *Dokl. Chem.*, 2001, **380**, 293–297.
17 B. H. Toby and R. B. Von Dreele, *J. Appl. Cryst.*, 2013, **46**, 544–549.
18 P. H. C. Eilers, *Analytical Chemistry*, 2003, **75**, 3631–3636.
19 P. H. C. Eilers, *Analytical Chemistry*, 2004, **76**, 404–411.
20 M. Newville, T. Stensitski, D. B. Allen and A. Ingargiola, *LMFIT: Non-Linear Least-Square Minimization and Curve-Fitting for Python*, 2014.
21 J. P. Perdew, K. Burke and M. Ernzerhof, *Phys. Rev. Letters*, 1996, **77**, 3865–3868.
22 G. Kresse and J. Furthmuller, *Phys. Rev. B*, 1996, **54**, 11169–11186.
23 ICDD, PDF-4+ 2019, 2019.
24 F. Colmenero, L. J. Bonales, J. Cobos and V. Timón, *Spectrochim. Acta Part A Mol. Biomol. Spectrosc.*, 2017, **174**, 245–253.
25 J. C. Taylor, *Acta Crystallographica Section B*, 1971, **27**, 1088–1091.
26 G. Lu, A. J. Haes and T. Z. Forbes, *Coord. Chem. Rev.*, 2018, **374**, 314–344.
27 E. Libowitzky, *Monatshefte fur Chemie*, 1999, **130**, 1047–1059.
28 Z. Urbanec and J. Cejka, *Collect. Czechoslov. Chem. Commun.*, 1979, **44**, 1–9.
29 R. L. Frost and J. Čejka, *J. Raman Spectrosc.*, 2007, **38**, 1488–1493.
30 J. I. Bullock, *J. Inorg. Nucl. Chem.*, 1967, **29**, 2257–2264.
31 T. M. Alam, Z. Liao, M. Nyman and J. Yates, *Journal of Physical Chemistry C*, 2016, **120**, 10675–10685.
32 I. Hamada, K. Lee and Y. Morikawa, *Phys. Rev. B*, 2010, **81**, 115452.
33 I. Hamada and S. Meng, *Chem. Phys. Let.*, 2012, **521**, 161–166.
34 A. G. Sowder, S. B. Clark and R. A. Fjeld, *Environ. Sci. Technol.*, 1999, **33**, 3552–3557.

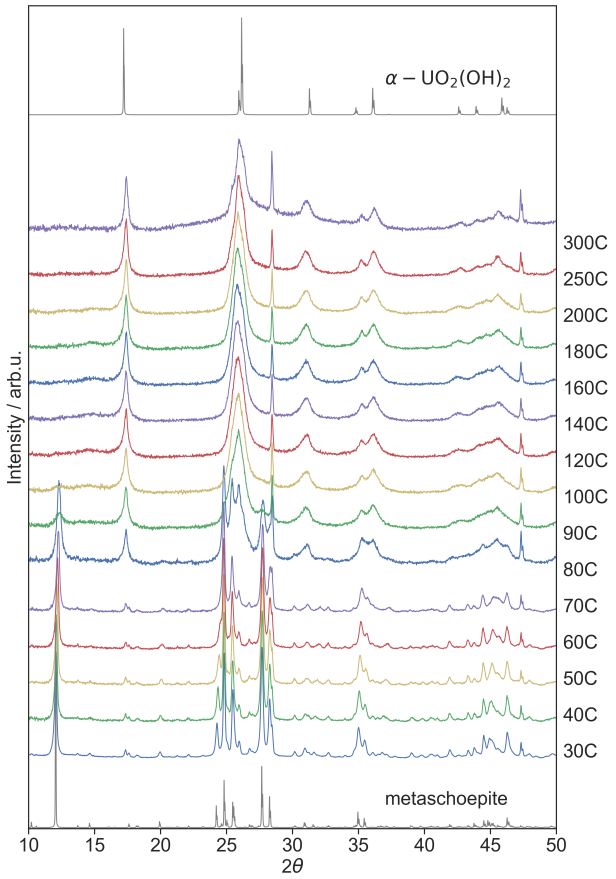

Fig. 18 XRD pattern (λ=1.5406 Å) of synthetic metaschoepite at increasing temperature, from 30 to 300 °C. The temperature was ramped 1 °C/min between scans, and the sample was equilibrated at each temperature for 30 min prior to data collection. Each XRD pattern was collected over 2 h. The expected patterns of metaschoepite[7] (PDF 04-011-3920[23]) and anhydrous uranyl hydroxide[25] (PDF 04-007-5373[23]) are shown for comparison.

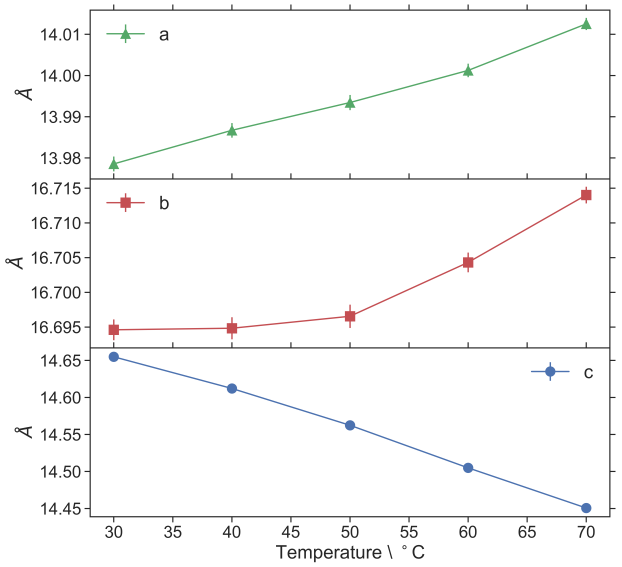

Fig. 19 Lattice parameters of synthetic metaschoepite between 30 and 70 °C, as determined via sequential Rietveld refinement.

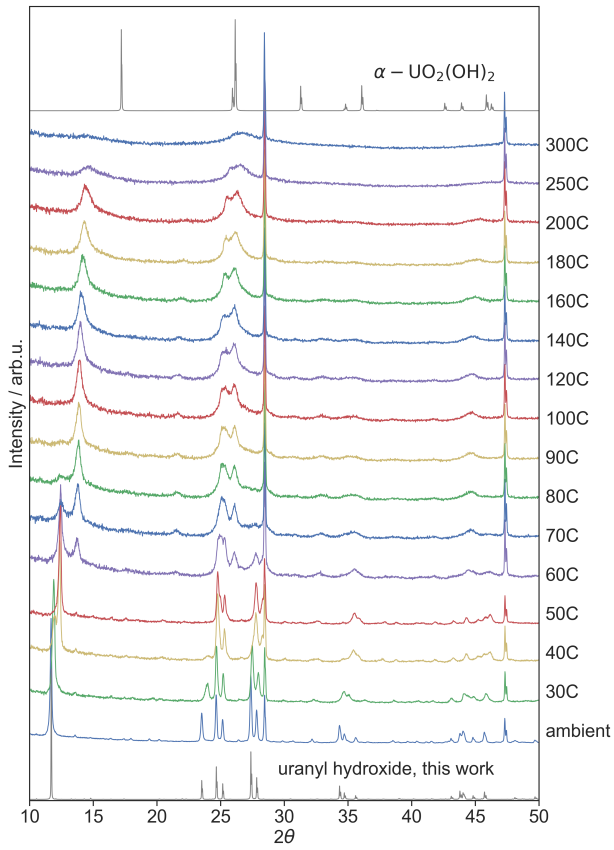

Fig. 20 XRD pattern (λ=1.5406 Å) of the uranyl hydroxide product at increasing temperature, from ambient to 300 °C. The temperature was ramped 1 °C/min between scans and the sample was equilibrated at each temperature for 30 min prior to data collection. Each XRD pattern was collected other 2 h. The previously determined expected pattern of the uranyl hydroxide product structure is shown for comparison, as well as that of anhydrous uranyl hydroxide[25] (PDF 04-007-5373[23]).

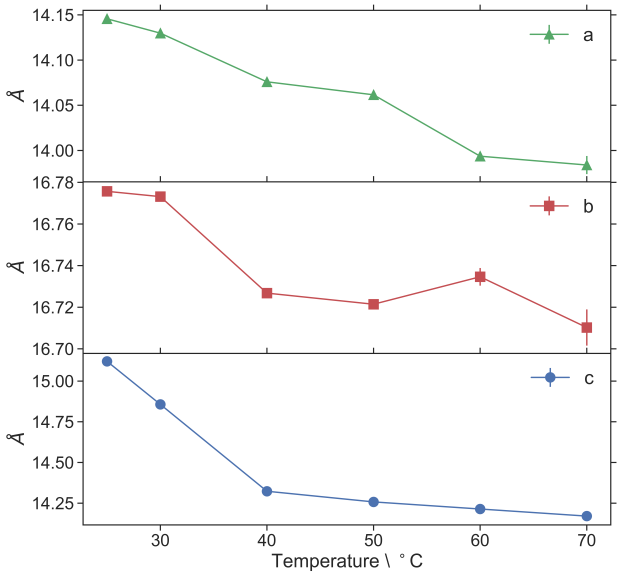

Fig. 21 Lattice parameters of the uranyl hydroxide hydration product between 30 and 70 °C, as determined via sequential Rietveld refinement.

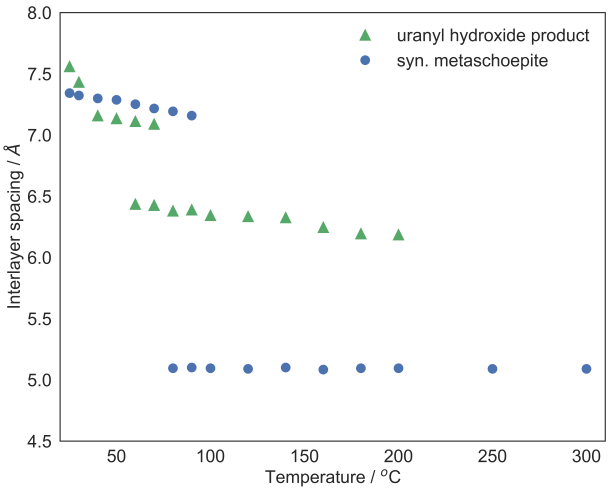

Fig. 22 Interlayer spacing of synthetic metaschoepite (blue circles) and the uranyl hydroxide product (green triangles), as determined by the position of the (002) reflection (or corresponding reflection in the anhydrous species), as a function of temperature. The spacing at each temperature was determined by the position of the (002) reflection (or (020) in anhydrous uranyl hydroxide, which is oriented with the uranyl layers normal to the *b*-direction[25]). In the cases where multiple (002)/(020) reflections were observed due to a phase mixture, both corresponding interlayer spacings are shown.

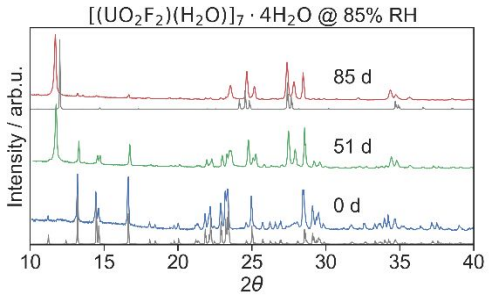

$[(UO_2F_2)(H_2O)]_7$*$4H_2O$ undergoes a transformation at high humidity to a novel uranyl hydroxide hydrate with structural similarities to schoepite and metaschoepite.